Available online at www.sciencedirect.com
SCIENCE DIRECT®
Electrochimica Acta 49 (2004) 1113–1125
ELECTROCHIMICA Acta
www.elsevier.com/locate/electacta

Enhanced corrosion resistance of AA 2024-T3 and hot-dip galvanized steel using a mixture of bis-[triethoxysilylpropyl]tetrasulfide and bis-[trimethoxysilylpropyl]amine

Danqing Zhu, Wim J. van Ooij*

Materials Sciences and Engineering Program, Department of Materials Science and Engineering, University of Cincinnati, Cincinnati, OH 45221-0012, USA

Received 6 May 2003; received in revised form 19 August 2003; accepted 26 October 2003

Abstract

The corrosion resistance of AA 2024-T3 and hot-dip galvanized steel (HDG) was studied after treatment with bis-[3-(triethoxysilyl)propyl] tetrasulfide (bis-sulfur silane), bis-[trimethoxysilylpropyl]amine (bis-amino silane), and their mixture. Electrochemical tests in neutral 0.6 M NaCl as well as scanning electronic microscopy (SEM)/energy-dispersive X-ray spectroscopy (EDX) were performed. The results showed that: (1) hydrophilic bis-amino silane did not offer good corrosion protection on either of the metals. This is probably because the bis-amino silane film tends to be positively charged. This promotes ingress of anions like Cl^- ions as well as water into the film by electrostatic attraction. As a result, corrosion readily proceeds at the interface. (2) Hydrophobic bis-sulfur silane performed very well on AA 2024-T3, but failed on HDG. The failure here stems from non-uniform film coverage on HDG owing to an insufficient wetting of bis-sulfur silane solution on the Zn oxide on HDG. Local corrosion initiates at defective sites which are poorly covered by the silane film. (3) A bis-sulfur/bis-amino mixture at the ratio of 3/1 greatly enhanced the corrosion resistance of both AA 2024-T3 and HDG. This substantial improvement is achieved by selectively overcoming the major shortcomings of the individual silanes.

Keywords: Surface treatment; Corrosion control; AA 2024-T3; HDG; EIS

1. Introduction

Silane surface treatment of metals has emerged in recent years as one of the promising alternatives for chromates in metal-finishing industries. Silanes are organofunctional hybrid organic–inorganic chemicals historically used as coupling agents for adhesion between organic and inorganic materials, such as glass fiber-reinforced polymeric composites [1–3]. A general silane structure is $(XO)_3Si(CH_2)_nY{\cdot}XO$ is a hydrolyzable alkoxy group which can be methoxy (OCH_3), ethoxy (OC_2H_5) or acetoxy ($OCOCH_3$). Y is an organofunctional group such as vinyl (C=C) or amino (NH_2) which is responsible for a good paint adhesion of a silane-treated metal surface.

Once hydrolyzed in an aqueous environment, such as water or water/alcohol mixture, alkoxy groups of the silane molecules convert to hydrophilic silanols (SiOH). These SiOH groups are readily absorbed onto a metal surface via formation of hydrogen bonds between SiOH groups and surface metal hydroxyls (MeOH) according to Fig. 1(a) [4]. In a subsequent curing or drying process, such bonds further convert to metallo-siloxane bonds (MeOSi) at the interface by releasing water, as shown in Fig. 1(b) [4]. Additionally, the excess SiOH groups on the metal surface also readily condense among themselves, forming a siloxane network (SiOSi) with an appreciable thickness on the metal surface. The as-formed SiOSi network is very hydrophobic if one of the substituents on the Si atom is a carbon atom [5].

The studies in terms of corrosion protection of metals by silanes started with some coupling agents mentioned above [6–13]. Over time, another group of silanes, also called "bis-silanes" with the general formula of $(XO)_3Si(CH_2)_n Y(CH_2)_nSi(XO)_3$ was found to perform much better than the

* Corresponding author. Tel.: +1-513-556-3194; fax: +1-513-556-3773.
E-mail address: vanooiwj@email.uc.edu (W.J. van Ooij).

0013-4686/$ – see front matter © 2003 Elsevier Ltd. All rights reserved.
doi:10.1016/j.electacta.2003.10.023

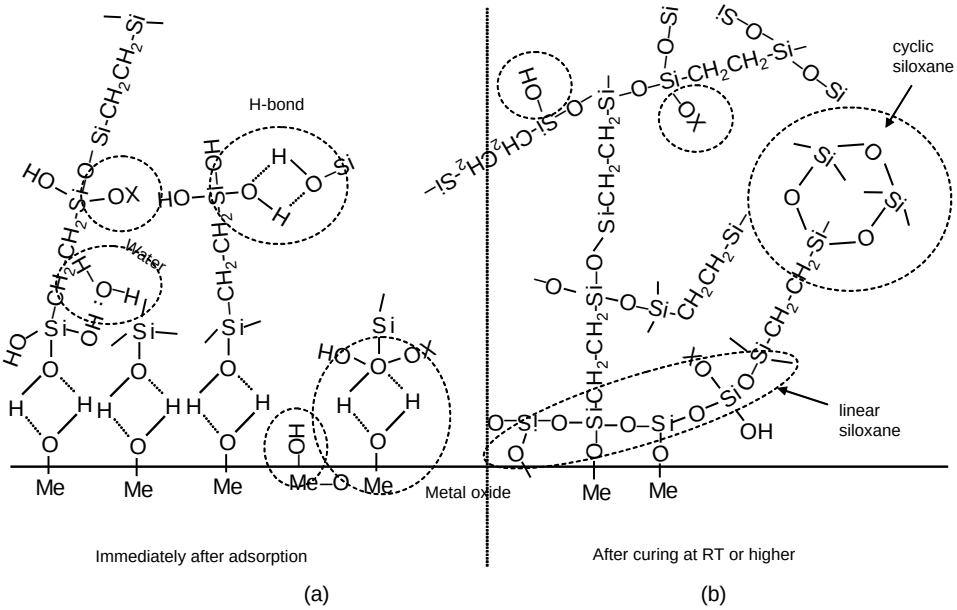

Fig. 1. Simplified schematic of bonding mechanism between silane molecules and metal surface hydroxide layer; (a) before condensation: hydrogen-bonded interface; and (b) after condensation: covalent-bonded interface [4].

above silane coupling agents, and thus, became a research focus in our laboratory. These "bis-silanes" have typically been used as crosslinkers for the coupling agents, examples of which include bis-[3-(triethoxysilylpropyl)]ethane (BTSE), bis-[3-(triethoxysilyl)propyl]tetrasulfide (bis-sulfur silane), and bis-[trimethoxysilylpropyl]amine (bis-amino silane), etc. [14–20]. Despite of their good corrosion protective ability, it was still observed that the performance of most bis-silanes is highly dependent upon the type and surface condition of the metal substrates. Bis-sulfur silane, for example exhibited good corrosion protection of Al alloys, it failed, however, when applied to hot-dip galvanized steel (HDG). This is surely not desirable for industries where metallic assembles or structures to be treated are made up of more than one metal. Therefore, our recent efforts were focusing on developing a universal silane system that should provide protectiveness for more than one metal. Preliminary work with a number of promising bis-silanes showed that a new silane mixture based on both bis-sulfur and bis-amino silanes performed extraordinarily well on both AA 2024-T3 and HDG in a salt immersion test. Unlike the individual silanes, the silane mixture of bis-sulfur and bis-amino silanes at a volume ratio of 3/1, survived a 0.6 M salt immersion test without severe pitting for AA 2024-T3 after 32 days of exposure, and for HDG after 8 days of exposure. The individual silanes, on the contrary, did not survive for both metals. Obviously, a certain synergic effect is generated by mixing these two individual silanes at certain optimum ratios, e.g. 3/1. This paper is devoted to understanding this synergic effect of the silane mixture on the corrosion protection of AA 2024-T3 and HDG by applying a variety of electrochemical tests and characterization tools such as scanning electronic microscopy (SEM) and energy-dispersive X-ray spectroscopy (EDX).

2. Experimental

2.1. Silanes

Bis-[3-(triethoxysilyl)propyl]tetrasulfide (or bis-sulfur silane) and bis-[3-(trimethoxysilyl)propyl]amine (bis-amino silane), with the trade names of Silquest A-1289® and Silquest A-1170®, respectively, were provided by OSi Specialties (Tarrytown, NY). Their purity was reported >95%. The chemical structures of these two silanes are given in Fig. 2.

2.2. Preparation of silane solutions

A 5% bis-sulfur silane water/alcohol solution was prepared by adding five parts of bis-sulfur silane into a mixture of de-ionized (DI) water and ethanol. The ratio of bis-sulfur silane/DI water/ethanol was 5/5/90 (v/v/v). The solution pH was 6.5. The solution was stirred for 10 min, and then aged in ambient conditions for at least 2 days to ensure that the silane molecules were sufficiently hydrolyzed so that enough SiOH groups were obtained for the subsequent condensation reactions [21]. A 5% bis-amino silane water/alcohol solution was made in a similar way. The ratio of bis-amino silane/DI water/methanol was 5/5/90 (v/v/v). The solution pH was lowered from its natural pH of 10.8 to 7.5 by adding acetic acid to enhance the solution stability [21]. The bis-amino silane solution was aged for 1 day before application. The 5% mixture solution was simply made by mixing the above

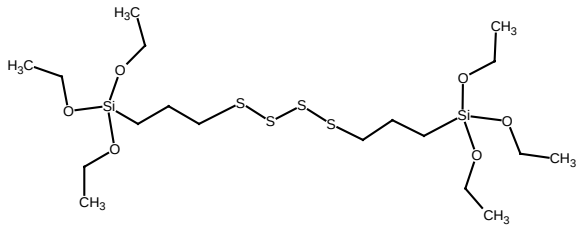

(a) Bis-[3-(triethoxysilyl)propyl]-tetrasulfide (bis-sulfur silane)

$(OC_2H_5)_3Si(CH_2)_3S_4(CH_2)_3Si(OC_2H_5)_3$

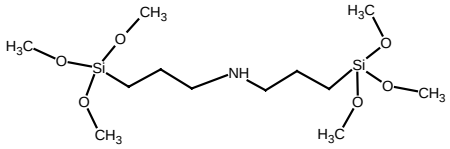

(b) Bis-[3-(trimethoxysilylpropyl)]amine (bis-amino silane)

$(OCH_3)_3Si(CH_2)_3NH(CH_2)_3Si(OCH_3)_3$

Fig. 2. Chemical structures and formulas of bis-sulfur silane (a); and bis-amino silane (b).

individual silane solutions at the bis-sulfur/bis-amino ratio of 3/1. The measured pH of the mixture was 7.5.

2.3. Surface cleaning and silane treatment

AA 2024-T3 and HDG panels (purchased from ACT Inc., Millsdale, MI) were alkaline cleaned in a 7.5% AC 1055® solution (provided by Lake Bluff, IL) at 70 °C for 5 min and rinsed with tap water. The panel surfaces should be thoroughly "water-break-free" at this point. The cleaned panels were dried using compressed air, and dipped into the silane solutions for 5–10 s. The silane-treated panels were again dried with compressed air to drive the alcohol out of the silane film, and followed by a 100 °C curing process for 24 h to extensively crosslink the silane films. It should be mentioned that curing the samples at 100 °C for 24 h is to obtain a fully-crosslinked silane film in a very short period (only for this study). As a matter of fact, 100 °C/24 h of curing is not used in practice. According to our previous studies [19], silane films also get crosslinked in the ambient or even during immersion in water. Only the processes take longer, compared to 100 °C/24 h. In practice, 10 min of curing at 100 °C for silane films that is used in the unpainted state, and no high temperature curing at all for those that will be used under paints.

2.4. Anodic and cathodic polarization tests

Anodic and cathodic polarization tests were carried out on AA 2024-T3 and HDG panels with and without the silane treatments in open-to-air 0.6 M NaCl solution at pH 6.5. The silane-treated panels were pre-immersed in the electrolyte for a certain period before data acquisition, i.e. 8 h for AA 2024-T3 and 3 h for HDG, in order to achieve a steady state. The bare panels were tested immediately after exposure to the electrolyte. A commercial saturated calomel electrode (SCE) and a platinum mesh were used as the reference and counter electrodes, respectively. The exposed area was 0.78 cm^2. On the average, five replicate samples were tested for each condition. The data were recorded from E_{corr}–0.50 V/SCE to E_{corr} (where, E_{corr} is corrosion potential of the tested samples) in the cathodic polarization tests, and from E_{corr} to E_{corr} + 0.50 V/SCE in the anodic polarization tests. The scan rate was 1 mV/s.

2.5. Electrochemical impedance spectroscopy measurements (EIS)

Electrochemical impedance spectroscopy measurements (EIS) were employed to monitor the corrosion performance of the silane-treated AA 2024-T3 and HDG systems as a function of immersion time in a 0.6 M NaCl solution (pH 6.5). The EIS measurements were carried out using an SR810 frequency response analyzer connected to a Gamry CMS100 potentiostat. The measured frequency range was from 10^{-2} to 10^5 Hz, with an AC excitation amplitude of 10 mV. SCE was used as the reference electrode and coupled with a graphite counter electrode. The surface area exposed to the electrolyte was 5.06 cm^2.

2.6. Ellipsometry

Ellipsometrmetric parameters, Psi, and Delta, were collected at 60, 65, 70, and 75° over a wide range of wavelengths from 300 to 800 nm. These values are angles for the complex value of the index of refraction at a smooth stainless steel (SS) substrate surface. A Cauchy model was used with the assumption that the optical properties of silane films are isotropic.

2.7. Surface energy measurement

The surface energies of the oxides on AA 2024-T3 and HDG were measured using VCA 2002 contact angle analyzer. The liquids, i.e. DI water and methylene iodide, were used for contact angle measurements. The harmonic mean method was employed for data processing.

3. Results and discussion

3.1. Silane film thickness measurements

Table 1 reports the film thickness of three silanes studied here. The silane films were deposited on a mirror-like stainless steel surface from their 5% silane solutions, and were cured at 100 °C for 1 h and aged in the ambient condition for 2 weeks. It is seen that the bis-amino silane film has the greatest film thickness value, i.e. 798.5 nm, among the three silanes, while the bis-sulfur silane film is the thinnest

Table 1
Film thickness of three silanes

Silane	Thickness (nm)	Non-uniformity (%)
Bis-sulfur silane (5%, ethanol-based, pH 6.5)	440.0	10
Bis-amino silane (5%, methanol-based, pH 7.5, adjusted by AC)	798.5	7
Mixture of bis-sulfur/bis-amino silane (or Mixture, 5%, 3/1, pH 7.5)	698.7	5

with the value of 440 nm. The mixture film has a thickness of 698.7 nm, i.e. between the two individual silane films. It is also noted that the bis-sulfur silane film gives the highest non-uniformity value of 10%, suggesting that the bis-sulfur silane film does not cover the substrate very homogenously, as compared to the others. Both bis-amino silane and the mixture films offer better film coverage on the substrate, as evidenced by the smaller non-uniformity values, i.e. 7 and 5%.

3.2. Electrochemical studies of silane-treated AA 2024-T3 and HDG in neutral 0.6 M NaCl

3.2.1. AA 2024-T3

Fig. 3(a) and (b) display the anodic and cathodic polarization behaviors of AA 2024-T3 treated with and without silanes measured in 0.6 M NaCl (pH 6.5) after 8-h exposure. It is seen in Fig. 3(a) that the current density for the untreated panel (curve 1) increases rapidly with applied voltages until the value of 10^{-2} A/cm^2 is reached, which reflects fast metal dissolution. After treated with bis-sulfur silane and the mixture (curves 3 and 4), the increase in the anodic current densities is largely slowed down. A nearly-potential-independent region is formed after 10^{-5} A/cm^2. This indicates that the extent of metal dissolution has been reduced by the silane deposition. A "zig-zag" region is seen for the bis-sulfur and the mixture at higher voltages (curves 3 and 4). Such "zig-zag" behavior is possibly related to silane film breakdown. The bis-amino silane, in contrast with the two above silanes, shows no suppression in the anodic current density (curve 2). This indicates that that the bis-amino silane film cannot provide sufficient corrosion protection for AA 2024-T3.

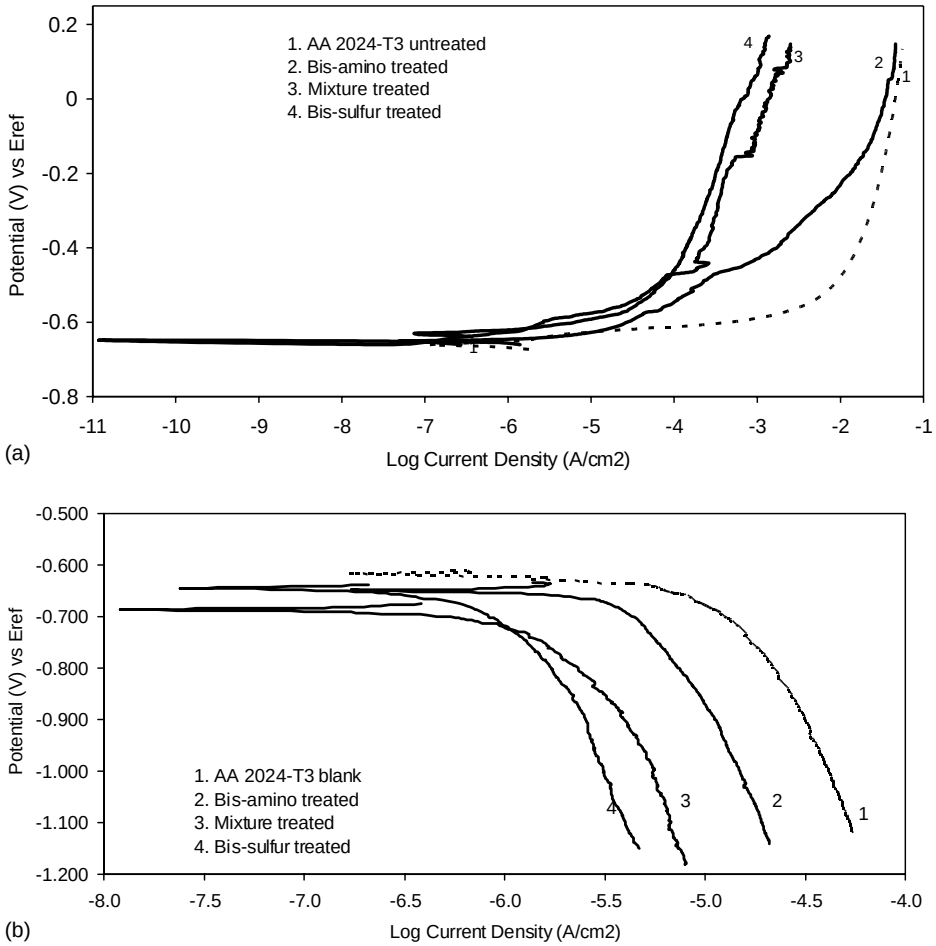

Fig. 3. DC polarization behaviors of AA 2024-T3 treated with and without silanes measured in 0.6 M NaCl (pH 6.5) after 8-h exposure, (a) anodic polarization; and (b) cathodic polarization.

The tested panel surfaces were visually inspected after the test ending at 0.2 V/SCE. Both untreated and bis-amino silane-treated surfaces extensively corroded, while the other two surfaces treated with the bis-sulfur silane and the mixture only showed a few tiny pits. This further supports that both bis-sulfur silane and the mixture offer good corrosion protection for AA 2024-T3, but not the bis-amino silane.

The cathodic behaviors of the three silane films (Fig. 3(b)) show a similar trend. The current densities for all silane-treated AA 2024-T3 panels shift to lower values compared to that for the untreated AA 2024-T3 (curve 1), with the shifts for the bis-sulfur and the mixture being the greatest extent (curves 3 and 4). The performance of the bis-amino silane, again, is inferior with respect to the other two silanes.

Since changes are not obviously seen in the curve shapes and the E_{corr} values for all samples in Fig. 3(a) and (b). It is, thus, concluded that the silanes deposited on AA 2024-T3 primarily perform as a physical barrier which retards electrolyte intrusion into the system.

The corrosion performance of the silane-treated AA 2024-T3 system in 0.6 M NaCl was examined using EIS. The EIS plots were obtained at the OCPs after 32 days of immersion, as shown in Fig. 4(a) and (b). The impedance behavior of the bis-sulfur and the mixture-treated AA 2024-T3 is comparable, with a high low-frequency impedance (Z_{lf}) values above $10^5\ \Omega$ (exposure area: 5.06 cm^2). The bis-amino silane, again, shows a poor performance. Its Z_{lf} value is nearly one order of magnitude lower than those of the bis-sulfur silane and the mixture. In the corresponding phase angle plot (Fig. 4(b)), two-time-constant behavior is observed for both bis-sulfur silane and mixture-treated AA 2024-T3 systems (curves 3 and 4), while only one time constant is seen for the bis-amino silane-treated and the bare AA 2024-T3 (curves 1 and 2). This two-time-constant-behavior for the bis-sulfur silane-treated AA 2024-T3 system was discussed previously [19,22]. According to these studies, the time constant at high frequencies ($\sim 10^4$ Hz) is attributed to the outermost bis-sulfur silane film, while the one at middle

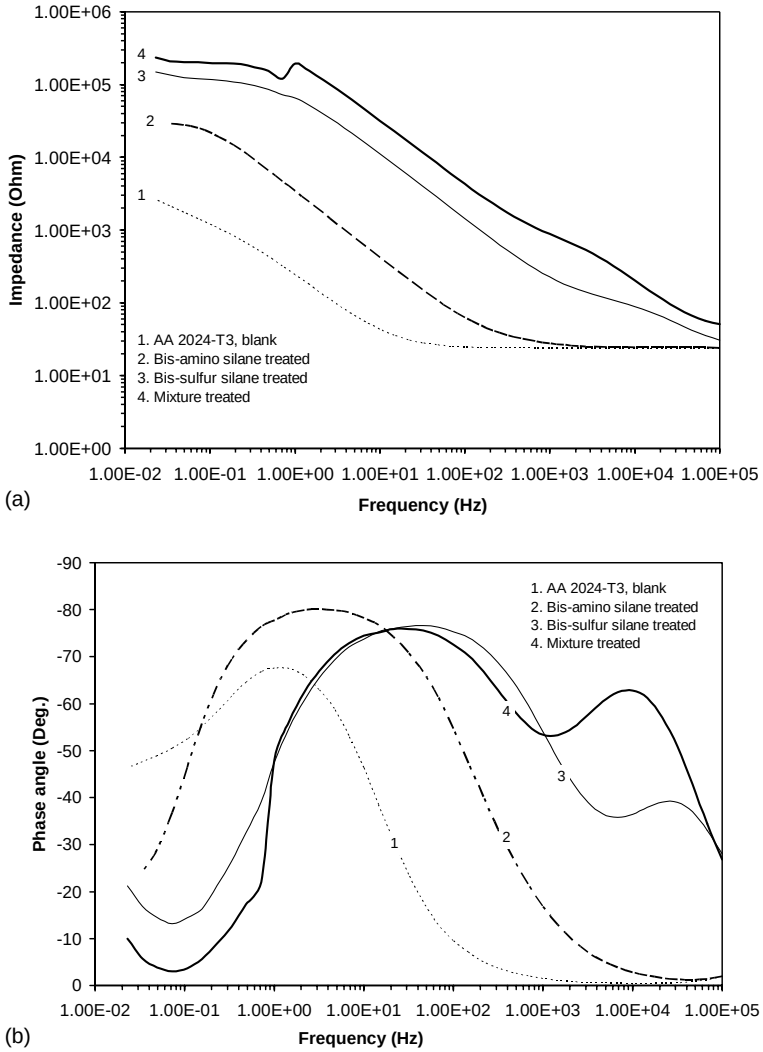

Fig. 4. Bode plots of silane-treated AA 2024-T3 panels in a 0.6 M NaCl solution (pH 6.5) after 32 days of exposure, (a) impedance plot; and (b) phase angle plot (exposed area: 5.06 cm^2).

frequencies (10 Hz) is due to an interfacial layer formed in the bis-sulfur silane-treated AA 2024-T3. The existence of this interfacial layer has been consistently confirmed in the previous EIS measurements as well as in SEM/EDX observations [19,22]. The mixture shows an EIS behavior similar to that of the bis-sulfur silane, suggesting that the mixture has a comparable performance and an analogous structure on AA 2024-T3 as the bis-sulfur silane. In the case of the bis-amino silane, one time constant centered at middle frequencies in Fig. 4 is also possibly due to the interfacial layer. The lack of impedance response for the outermost bis-amino silane film is most likely related to its hydrophilic nature that highly promotes water/ion penetration. More details regarding this aspect will be discussed later.

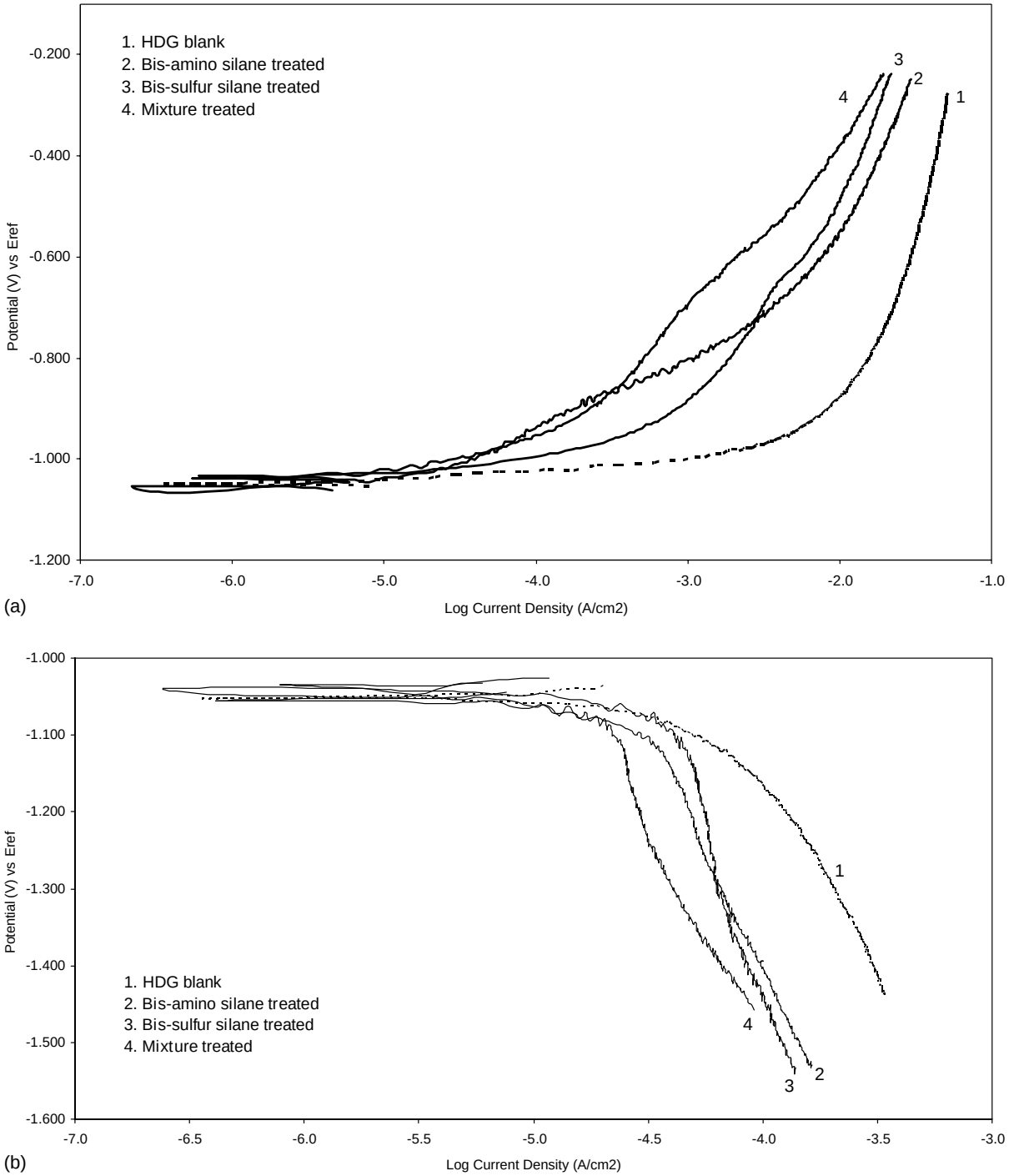

Fig. 5. DC polarization curves of silane-treated HDG panels, measured in 0.6 M NaCl solution (pH 6.5) after 3 h of exposure, (a) anodic polarization; and (b) cathodic polarization.

3.2.2. HDG

Fig. 5(a) and (b) show anodic and cathodic polarization curves of HDG treated with and without the silanes, obtained in 0.6 M NaCl (pH 6.5) after 3 h of exposure to the electrolyte. In Fig. 5(a), the anodic current density for the bare HDG increases rapidly, followed by a nearly potential-independent region after achieving 10^{-2} A/cm^2 (curve 1). This indicates that the Zn coating on HDG initially experiences heavy dissolution. The further dissolution slows down after 10^{-2} A/cm^2, due to the hindrance effect of the corrosion products built up in-situ. The anodic current densities for all silane-treated samples have been reduced to different extents. The mixture performs the best among them, giving considerable suppression (curve 4) soon after

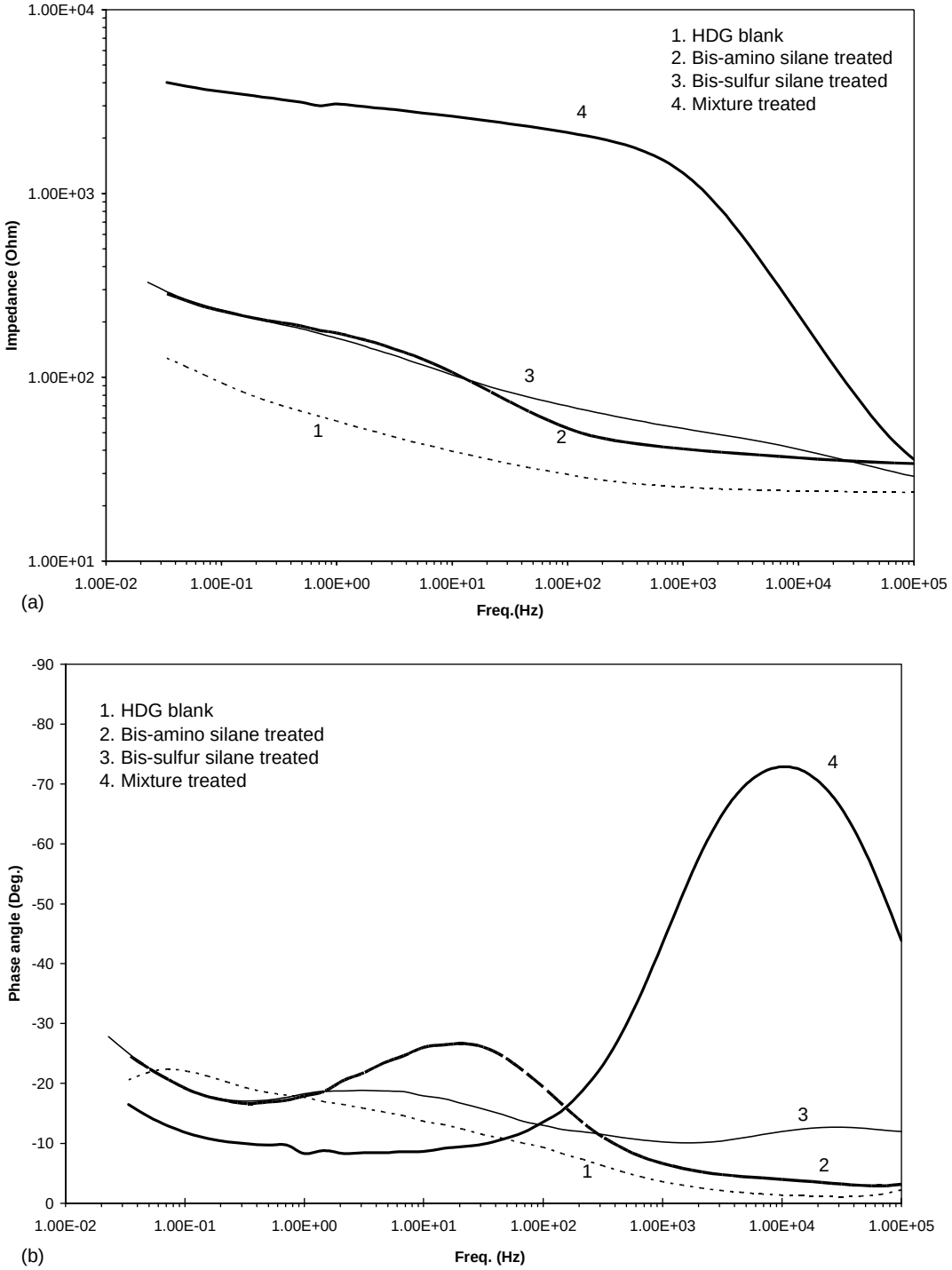

Fig. 6. Bode plots of silane-treated HDG panels measured in 0.6 M NaCl solution (pH 6.5) after 8 days of exposure, (a) impedance plot; and (b) phase angle plot (exposed area: 5.06 cm^2).

Fig. 7. AA 2024-T3 panels after 32 days of immersion in 0.6 M NaCl solution, (a) untreated; (b) bis-sulfur silane-treated; (c) mixture-treated; and (d) bis-amino silane-treated.

the value of 10^{-4} A cm^2 is reached. Both bis-sulfur and bis-amino silanes show a certain degree of inhibition (curves 2 and 3), yet their inhibitive effect is not as pronounced as that of the mixture (curve 4).

Cathodic behaviors of the above HDG panels after exposed for 3 h in the same electrolyte are presented in Fig. 5(b). Again, the mixture (curve 4) among all three silanes exhibits the best corrosion protection performance by reducing the cathodic current density to the greatest extent. Bis-sulfur and bis-amino silanes perform similarly in this case (curves 2 and 3), i.e. inferior compared to the mixture.

EIS results after 8-day immersion are compared in Fig. 6(a) and (b). It is seen in Fig. 6(a) that, among all silanes, only the mixture-treated HDG system retains a much higher Z_{lf} value than the others after 8 days of immersion. The Z_{lf} values for both bis-sulfur and bis-amino silanes are similar, i.e. approximately one order of magnitude lower than that of the mixture. This is consistent with the result from the above DC polarization tests, showing that the mixture is a better solution for corrosion protection of HDG than the individual silanes. It is also noted that in the corresponding phase angle plot (Fig. 6(b)), the mixture shows a pronounced time constant with its maximum peak located at about −75° at high frequencies, while the phase angle plots for the others are almost flattened after 8 days of immersion, showing little protectiveness for HDG. Unlike the mixture-treated AA 2024-T3 system which exhibits two time constants (in Fig. 4(b)), only one time constant is shown for the mixture-treated HDG. This indicates that rather than forming two distinct layers (i.e. outermost silane layer and interfacial layer) as in the case of AA 2024-T3, the mixture only forms one single structure with HDG that is detectable to EIS.

Figs. 7 and 8 present the scanned images of both silane-treated AA 2024-T3 and HDG panels after the EIS

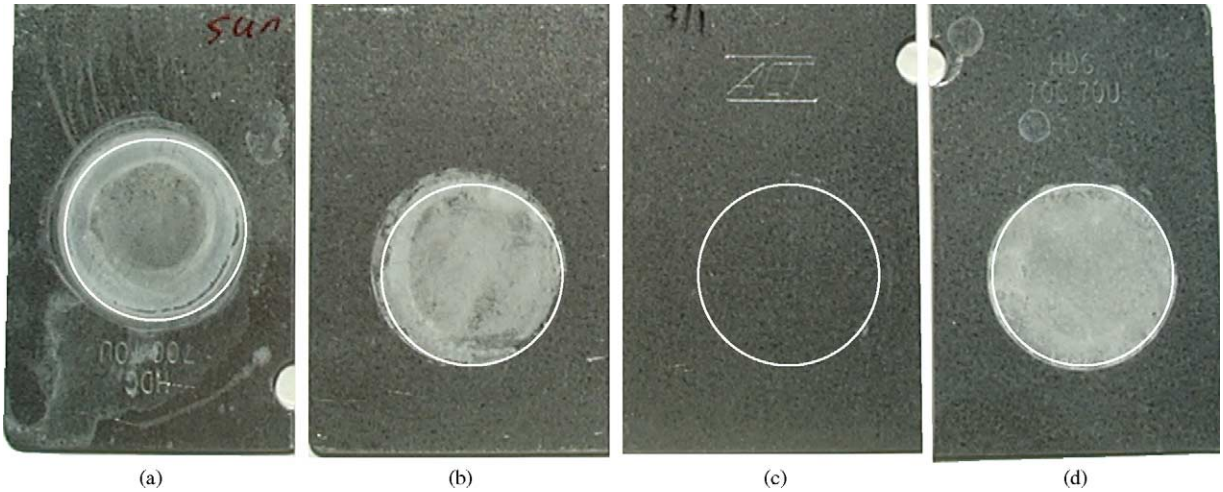

Fig. 8. HDG panels after 8 days of immersion in 0.6 M NaCl solution, (a) untreated; (b) bis-sulfur silane-treated; (c) mixture-treated; and (d) bis-amino silane-treated.

measurements. It is clearly seen that no corrosion is shown on both mixture-treated AA 2024-T3 and HDG panels (Figs. 7(c) and 8(c)), indicating that the mixture provides good corrosion protection for both metals. The bis-sulfur silane, although, it performs similarly as the mixture on AA 2024-T3 (Fig. 7(b)), perform poorly on HDG (Fig. 8(b)). The bis-amino silane consistently exhibits its poor corrosion performance on both alloys, i.e. large pitting patches on AA 2024-T3 (Fig. 7(d)) and uniform corrosion on HDG (Fig. 8(d)). Based upon the above results, the silanes can, thus, be ranked as follows in terms of their protective efficiency on AA 2024-T3 and HDG (from the best to the worst): mixture (bis-sulfur/bis-amino = 3/1) > bis-sulfur silane > bis-amino silane.

3.3. SEM observation of silane-treated AA 2024-T3 and HDG surfaces after immersion in neutral 0.6 M NaCl

In this section, we are attempting to understand the corrosion mechanisms for all silane-treated systems from a microstructure point of view. Prior to SEM and EDX examination, all samples were exposed to a neutral 0.6 M NaCl solution for various times to initiate pits, i.e. 15 days for AA 2024-T3 and 5 days for HDG.

3.3.1. AA 2024-T3

The SEM images of pitting areas on the silane-treated AA 2024-T3 surfaces after immersion are shown in Fig. 9(a)-(c). Similar features are seen for all pitted areas on these three silane-treated surfaces. Three distinct regions are identified for all the samples, indicated as regions A, B, and C in the figures. Obviously, region A is the silane-coated area where the substrate is still covered continuously with the intact silane film. Region B is the unattacked area from which the top layer of silane film has been delaminated. It is noted that some micro-cracks are formed in region A that is adjacent to region B. The formation of these micro-cracks was primarily caused by film swelling during immersion [22]. Region C shows a heavily corroded area, where the metal has been eaten away. EDX identification of these three regions for all silane-treated AA 2024-T3 panel surfaces is listed in Table 2.

It is seen in Table 2 that the compositions of regions A and B are analogous for all silanes: both regions are featured with a higher amount of Si, varying from 2.3 to 8.8 wt.%, with respect to bare AA 2024-T3. Such a high content of Si detected in region B strongly suggests that region B is not simply the bare AA 2024-T3 substrate (nominally contains 0.5 wt.% of Si [23]) exposed after the delamination of the uppermost part of the silane film, but is probably a new structure, the so-called interfacial layer, formed between the

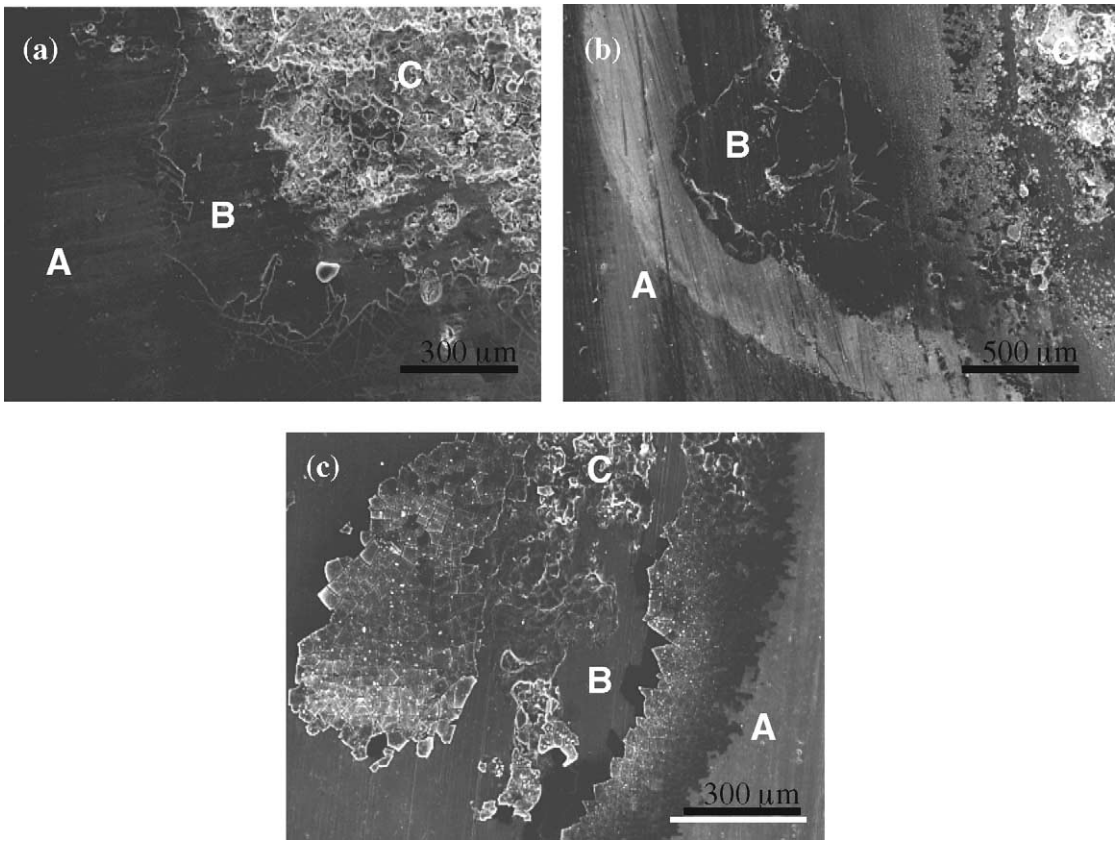

Fig. 9. SEM images of silane-treated AA 2024-T3 surfaces after 32 days of immersion in a 0.6 M NaCl solution at pH 6.5, (a) bis-sulfur silane-treated [27]; (b) bis-amino silane-treated; and (c) mixture-treated.

Table 2
Compositions of three regions in the silane-treated AA 2024-T3 systems

Element	Region A			Region B			Region C			AA 2024-T3 [23]
	Bis-sulfur	Bis-amino	Mix	Bis-sulfur	Bis-amino	Mix	Bis-sulfur	Bis-amino	Mix	
O	8.0	13.3	12.3	6.7	9.6	5.1	43.0	34.3	22.4	–
Mg	1.3	1.0	1.5	1.2	1.0	0.9	–	–	–	1.2–1.8
Al	81.4	70.8	71.5	74.2	74.8	77.4	28.5	53.3	67.5	Rem
Si	2.7	8.5	6.6	7.1	8.8	8.0	–	4.4	0.7	0.5
S	2.3	–	4.4	6.2	–	4.6	–	–	–	–
Cl	–	1.6	–	0.5	1.2	–	0.8	1.0	–	–
Cu	4.3	4.8	3.7	4.1	4.6	3.9	27.5	6.7	9.0	3.8–4.9

bis-sulfur silane and the substrate. Indeed, this interfacial layer was first detected as an additional time constant (RC3) appearing in various curing processes in the previous EIS studies [19,21]. This interfacial layer is thought to consist of SiOSi and SiOAl bonds formed via condensation reactions among SiOH groups themselves and between SiOH and AlOH groups. It was further suggested [22] that the highly crosslinked interfacial layer rather than the outermost silane film is a major contributor in corrosion protection of AA 2024-T3. The interfacial layer anchors tightly to the AA 2024-T3 substrate due to a high density of AlOSi bonds formed at the interface. In addition, AlOSi bonds are formed by the consuming of hydrophilic AlOH groups at the metal surface. The metal surface is, thus, no longer favorable for water adsorption, and consequently the tendency for aqueous corrosion of the metal is suppressed.

Although, corrosion inhibition of the metal is intimately related to the formation of AlOSi bond, the bond itself is not hydrolytically stable [1]. When exposed to a large amount of water, the AlOSi bond is hydrolyzed back to reform hydrophilic AlOH groups and SiOH groups. This obviously destroys the hydrophobicity of the metal surface. Therefore, suppression of water uptake in a silane film is of virtual importance in terms of maintaining a good adhesion between the silane film and the substrate. In general, there are two major methods which can be employed to enhance water resistance of the film. (1) Fully crosslinking of silane films. On one hand, film porosity is reduced by crosslinking; on the other hand, a hydrophobic SiOSi network is built up by consuming hydrophilic SiOH groups. (2) Enhancing intrinsic film hydrophobicity by employment of silanes with hydrophobic organic–inorganic substitutions such as the sulfur chain ($–S_4–$) in bis-sulfur silane and alkyl groups ($–(CH_2)_2–$) in BTSE. With the enhancement of water resistance of the silane film, water uptake in the film is suppressed and hydrolysis of AlOSi bond is prevented. The corrosion protection of the metal is, therefore, guaranteed.

Another important effect shown in Table 2 is that a noticeable amount of chloride was detected for regions A and B in the bis-amino silane-treated AA 2024-T3 system, i.e. 1.6 wt.% in region A and 1.2 wt.% for region B. Such a high amount of chloride, however, was not found for the bis-sulfur silane and the mixture treated AA 2024-T3 surfaces. This finding reveals the cause behind the inferior performance of the bis-amino silane film. It is commonly known that the secondary amino groups (–NH–) in the bis-amino silane tend to protonate in the presence of water. The protonation can be expressed as below [24]

$$–NH– + H_2O \rightleftarrows –NH_2^+– + OH^- \quad (1)$$

$–NH_2^+–$ groups are formed, releasing hydroxide ions (OH^-) as the byproduct. This effect actually explains why the bis-amino solution is highly alkaline, with a natural pH ~10.8. Since the silane solution tends to gel at such high pH in a few minutes, acetic acid (HAc) is added into the bis-amino solution to reduce the pH to 7 to stabilize the solution. When a metal is treated with the bis-amino silane water/alcohol solution, the as-formed silane film on the metal is positively-charged due to these $–NH_2^+–$ groups. Upon exposing to a NaCl solution, the positively-charged bis-amino silane film will electrostatically attract anions like Cl^- ions as well as water into the film, as illustrated in Fig. 10. Corrosion occurs at the metal surface once a sufficient amount of Cl^- ions/water arrives. A similar observation for γ-APS was discussed elsewhere [6,15]. The electrostatic attraction of SO_4^- ions by the bis-amino silane film was also reported elsewhere [21].

Indeed, the absence of the time constant at high frequencies for the bis-amino silane film in Fig. 4(b) is also related to its hydrophilic structure. That is, electrolyte intrusion into the hydrophilic outermost bis-amino silane film is so fast that no corresponding impedance response is detectable to EIS. In other words, the top part of the film is “transparent” in EIS.

Another piece of evidence exists which strongly supports the above view. When further neutralizing OH^- ions with HAc in the bis-amino silane solution (i.e. further decreasing the solution pH), reaction equilibrium (1) is driven to right. More –NH– groups are expected to be protonated. As a result, the as-formed bis-amino silane film should be more highly positively charged or more hydrophilic as compared to the one formed from the pH 7 solution. Fig. 11(a) shows the SEM image of an AA 2024-T3 sample treated with a 5% bis-amino silane solution at pH 4, after 4 days of immersion in neutral 0.6 M NaCl. Unlike the bis-amino silane film in Fig. 9(b), the entire bis-amino silane film has uniformly

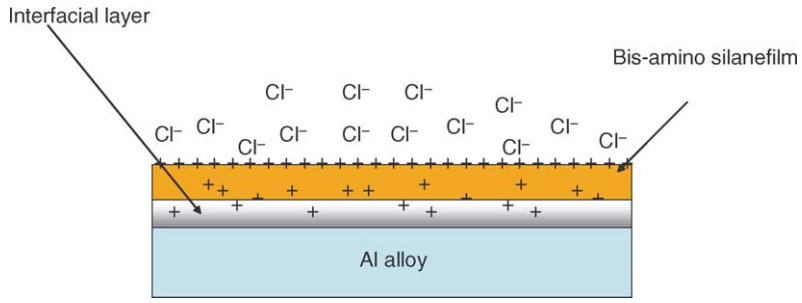

Fig. 10. Attraction of Cl^- ions in the electrolyte by a positively-charged bis-amino silane-treated alloy.

cracked into small pieces, spreading all over the alloy surface. Fig. 11(b) gives the EDX spectrum of the piece "A" in Fig. 11(a). Again, a high amount of Cl is observed here, indicating a strong attraction of Cl^- ions into the film. Apparently, the bis-amino silane film was heavily swollen by the electrolyte intrusion during immersion, which resulted in severe film cracking upon subsequent drying shown in Fig. 11(a).

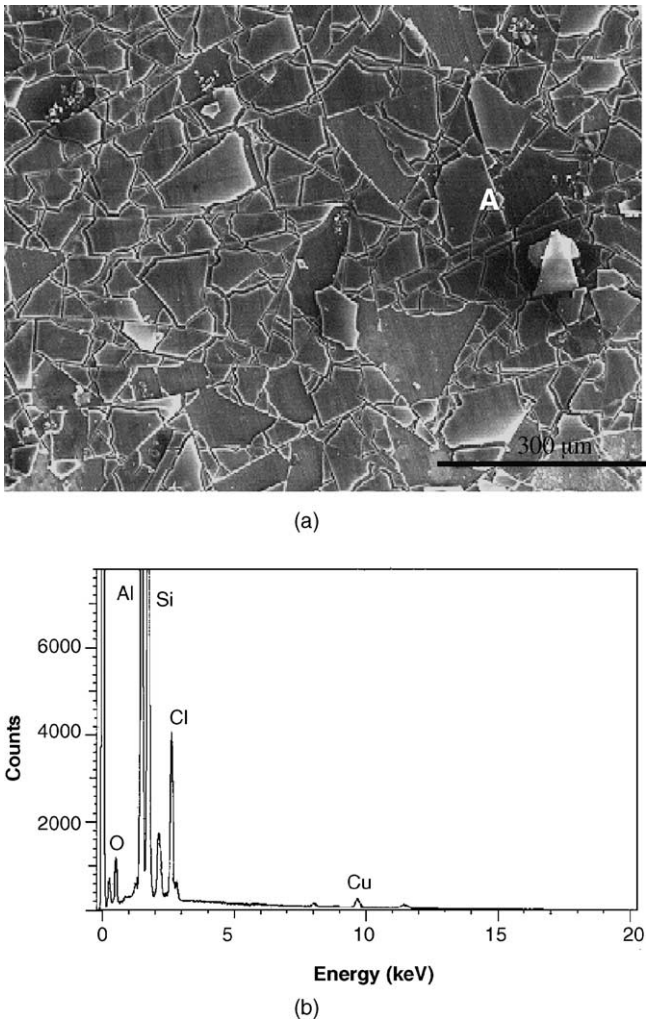

Fig. 11. Bis-amino silane-treated AA 2024-T3 (in 5% bis-amino silane solution at pH 4), after immersion in 0.6 M NaCl solution (pH 6.5) for 4 days, (a) SEM image; and (b) EDX spectrum of bis-amino silane piece (site A in Fig. 11(a)).

The bis-sulfur silane film, on the contrary, is neutral and is not expected to promote ingress of Cl^- ions/water. Therefore, no chloride content was detected. As for the mixture (bis-sulfur/bis-amino = 3/1), although, it also contains some amount of $–NH_2^+–$ groups, no chloride signal was detected in the EDX analysis. This suggests that the number of $–NH_2^+–$ in the mixture film is so low that its attraction to Cl^- ions can be negligible. In other words, the film of the mixture is hydrophobic enough to avoid promoting the transport of Cl^- ions/water, which now behaves similarly to the bis-sulfur silane. Thus, both bis-sulfur silane and the mixture films provide equally good protectiveness on AA 2024-T3.

3.3.2. HDG

Fig. 12 shows the SEM images of silane-treated HDG surfaces after immersion in a neutral 0.6 M NaCl solution for 5 days. The EDX results are presented in Tables 3–5. It is clearly seen in Fig. 12 that the morphologies of all three silane-treated HDG surfaces are distinctly different.

In Fig. 12(a), clusters of corrosion products are observed here and there on the bis-sulfur silane-treated HDG surface, along with irregular dark patches distributed uniformly over the surface. The EDX results of these dark patches in

Table 3
Compositions of bis-sulfur silane-treated HDG, shown in Fig. 12(a)

Element	Grey region	Dark patch	Corroded region
O	6.7	8.7	35.8
Si	5.2	17.8	0.7
S	5.4	24.1	–
Cl	–	–	1.4
Zn	82.7	49.1	62.0

Table 4
Compositions of bis-amino silane-treated HDG, shown in Fig. 12(b)

Element	Intact region	Corroded region
O	8.9	39.8
Si	11.6	0.6
Cl	1.7	3.2
Zn	77.8	56.3

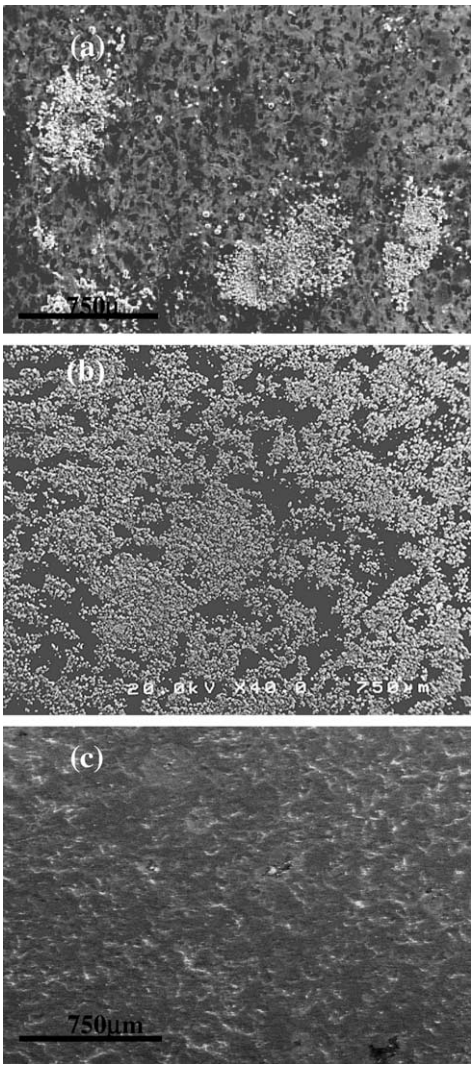

Fig. 12. SEM images of silane-treated HDG surfaces after 8 days of immersion in a 0.6 M NaCl solution at pH 6.5, (a) bis-sulfur silane-treated; (b) bis-amino silane-treated; and (c) mixture-treated.

Table 3, compared to the other regions or grey region, show markedly high amounts of S (24.1 wt.%) and Si (17.8 wt.%) and relatively low content of Zn (49.1 wt.%). It is also noted that the S/Si ratio is similar for both dark patches and the other regions in Fig. 12(a). Therefore, the dark patches are very likely the areas of thicker bis-sulfur silane films. In other words, HDG surface is not uniformly covered with the bis-sulfur silane film. Such phenomenon, however, was not observed for the bis-sulfur treated AA 2024-T3 surface. This difference could be explained in light of different wettabilites of aluminum and zinc oxides. It is seen in Table 6 that aluminum oxide on AA 2024-T3 has a higher surface energy of 73.9 mJ/m^2 than 54.6 mJ/m^2 of Zn oxide on HDG. It is known that for a given solution, a metal with higher surface energy is expected to have a better wetting of the solution. In the case of bis-sulfur silane solution, the wetting of Al oxide by the bis-sulfur silane solution should not be a problem. However, the same bis-sulfur silane solution seems too hydrophobic to the Zn oxide that has a lower surface energy. This obviously leads to an insufficient wetting of the Zn oxide. As a result, a non-homogeneous bis-sulfur silane layer is formed on HDG, as shown schematically in Fig. 13. Local corrosion initiates at those defective sites that are poorly covered by the bis-sulfur silane film.

Table 5
Compositions of mixture silane-treated HDG, shown in Fig. 12(c)

Element	Region 1	Region 2
O	6.2	5.8
Si	8.3	9.0
S	5.6	6.8
Cl	–	–
Zn	79.8	78.3

Table 6
Surface energies of oxides on AA 2024-T3 and HDG

Alloy	Surface energy (mJ/m^2)
AA 2024-T3	73.9
HDG	54.6

As opposed to the bis-sulfur silane, the bis-amino silane is more hydrophilic and should wet the Zn oxide readily, forming a uniform silane film on HDG. Nevertheless, the hydrophilic nature of the bis-amino silane film still leads to heavy corrosion on HDG (Fig. 12(b)). This is indeed confirmed by a noticeable amount of Cl (1.7%) detected in the bis-amino silane film on HDG (Table 4).

Fig. 12(c) shows the SEM image of an intact mixture-treated HDG surface where no corrosion was observed after 5 days of immersion. Neither dark patches nor chloride signal are discerned on this sample. Two regions were chosen randomly on the surface for compositional identification by EDX. The EDX results are shown in Table 5. The compositions of both regions can be considered as the same within the experimental variations, indicating that the mixture gives a uniform film coverage on HDG as the bis-amino silane does. Apparently, with the addition of a small amount of bis-amino silane, the solution of the bis-sulfur/bis-amino silane mixture becomes hydrophilic enough to wet the Zn oxide and consequently form a homogeneous film. It is evidenced in Fig. 12(c) that such film still offers good corrosion protection on HDG, inferring that the as-formed mixture film is hydrophobic enough from a corrosion protection

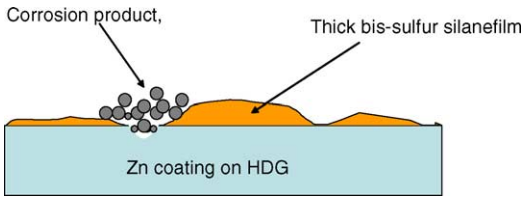

Fig. 13. Poorly-coated HDG surface with a bis-sulfur silane layer, and local corrosion occurring at defects.

perspective. The hydrophobicity of the mixture film is obviously attributed to the large amount of bis-sulfur silane in the mixture. In all, the mixture film provides a universal protection on both AA 2024-T3 and HDG by selectively overcoming the major drawbacks of the two individual silanes.

4. Conclusions

1. Hydrophilic bis-amino silane film consistently showed an inferior corrosion protection performance on AA 2024-T3 and HDG. This is because the bis-amino silane film is positively-charged due to the protonation of the secondary amino groups. This positively-charged bis-amino silane film strongly attracts anions such as Cl^- ions as well as water from the environment, eventually leading to corrosion of the metal substrates, as the MeOSi bonds will be destroyed by the water/Cl^- ions ingress.
2. Hydrophobic bis-sulfur silane performed very well on AA 2024-T3, but failed on HDG. It was found that the major cause behind this failure is the insufficient wetting of the bis-sulfur silane solution towards the Zn oxide on HDG, which results in non-uniform film coverage on HDG. Corrosion starts at defective sites where are poorly covered by the film.
3. A mixture at the bis-sulfur/bis-amino ratio of 3/1 enhances the corrosion resistance of both AA 2024-T3 and HDG. This improvement is achieved for the mixture by selectively overcoming the major drawbacks of the two individual silanes. A small portion of bis-amino silane makes the mixture solution hydrophilic enough to wet Zn oxide on HDG, which facilitates the formation a homogenous film on HDG. On the other hand, a large portion of bis-sulfur silane enhances the hydrophobicity of the mixture film, which is the basis for good protective performance of the mixture.

Acknowledgements

The authors gratefully acknowledge the financial support for this work by the Air Force Office of Scientific Research under contract F49620-01-1-0352. The authors would also wish to thank Matt Stacy for ellipsometry measurements, Srinivas Subramaniam and Marty Pluth for SEM/EDX operation and Robert Layman of AST Products Inc. for the assistance of surface energy measurements.

References

[1] E.P. Plueddemann, Silane Coupling Agents, second ed., Plenum Press, New York, 1991.
[2] K.L. Mittal (Ed.), Silanes and Other Coupling Agents, VSP, Utrecht, 1992.
[3] K L. Mittal (Ed.), Silanes and Other Coupling Agents, vol. 2, VSP, Utrecht, 2000.
[4] V. Palanivel, D. Zhu, W.J. van Ooij, Prog. Org. Coat., 2003.
[5] W.J. van Ooij, M. Stacy, V. Palanivel, A. Lamar, D. Zhu, The Use of Organofunctional Silanes as a Major Constituent in Organic Coatings for enhanced Corrosion Protection, ASM Meeting, October, Columbus, OH, 2002.
[6] M.A. Petrunin, A.P. Nazarov, Yu.N. Mikhailovski, J. Electrochem. Soc. 143 (1996) 251.
[7] A.M. Beccaria, L. Chiaruttini, Corros. Sci. 41 (1999) 885.
[8] P.R. Underhill, D.L. Duquesnay, Corrosion resistance imparted to alminum by silane coupling agents, in: K.L. Mittal (Ed.), Silanes and Other Coupling Agents, vol. 2, VSP, Utrecht, 2000, p. 149.
[9] Z. Pu, W.J. van Ooij, J.E. Mark, J. Adhes. Sci. Technol. 11 (1997) 29.
[10] W.J. van Ooij, A. Sabata, J. Adhes. Sci. Technol. 5 (1991) 843.
[11] C. Zhang, Ph.D. Dissertation, Department of Materials Science and Engineering, University of Cincinnati, 1997.
[12] S.E. Hörnström, J. Karlsson, W.J. van Ooij, N. Tang, H. Klang, J. Adhes. Sci. Technol. 10 (1996) 883.
[13] W. Yuan, W.J. van Ooij, J. Colloid Interf. Sci. 185 (1997) 197.
[14] W.J. van Ooij, T.F. Child, CHEMTECH 28 (1998) 26.
[15] V. Subramanian, W.J. van Ooij, Corrosion 54 (1998) 204.
[16] G.P. Sundararajan, M.S. Thesis, Department of Materials Science and Engineering, University of Cincinnati, 2000.
[17] W.J. van Ooij, D. Zhu, G.P. Sundararajan, S.K. Jayaseelan, Y. Fu, N. Teredesai, Surf. Eng. 16 (2000) 386.
[18] D. Zhu, Ph.D. Dissertation, Department of Materials Science and Engineering, University of Cincinnati, 2003, submitted for publication.
[19] W.J. van Ooij, D. Zhu, Corrosion 157 (5) (2001) 413.
[20] W.J. van Ooij, D. Zhu, V. Palavinel, A. Lamar, M. Stacy, Silicon Chem., in press.
[21] D. Zhu, W.J. van Ooij, J. Adhes. Sci. Technol 16 (1) (2002) 1235.
[22] D. Zhu, W.J. van Ooij, Corros. Sci. (2003) 2177.
[23] D.A. Jones, Principles and Prevention of Corrosion, second ed., Prentice-Hall, 1996, 45 (10) p. 556.
[24] M. Hein, L. Best, College Chemistry: an Introduction to Inorganic, Organic and Biochemistry, second ed., Brooks/Cole Publishing Co., CA, 1990.